Incoherent change detection using amplitude sidescan sonar images

Isabelle Quidu

INCOHERENT CHANGE DETECTION USING AMPLITUDE SIDESCAN SONAR IMAGES

I. Quidu   ENSTA Bretagne, STIC/OSM, Lab-STICC UMR CNRS 6285, 2 rue François Verny, 29806 Brest Cedex 9, France

1   INTRODUCTION

The automatic detection of temporal changes in sonar images is of high interest for monitoring critical areas as ports or channels used by submarines for instance. This problem is addressed here as incoherent change detection between two sonar passes.

To be able to compare two surveys, sonar images have first to be registered to each other. A global translation between the master image and the slave image has been estimated here at a coarse-to-fine image resolution by minimizing the Kullback-Leibler divergence between the first and the second sets of amplitude distributions related to homogeneous areas of the master image. This is detailed in section 2.

Then two different methods for the detection of changes in terms of contacts in the common area of the registered images are proposed in section 3. The first method is one of the well-known techniques used for synthetic aperture radar imagery: the log ratio of images. The second one is made of two stages: firstly a goodness-of-fit test is applied to every image divided into small overlapped snippets in order to detect statistical deviations due to possible contacts; secondly a pixelwise difference is simply performed between two images whose detected snippets have been put in a non-zero pixel value. For both methods morphological operations and local correlations have been performed in order to discard false alarms.

Advantages and drawbacks of the two proposed methods are discussed in section 4 with results on a set of data collected by Defence R&D Canada Atlantic with a high-frequency sidescan sonar a month apart in the winter of 2008 in a port area.

2   RIGID-BODY REGISTRATION FOR SONAR IMAGES

2.1   Previous work

Sonar images registration has been widely studied in the 2000s. Proposed methods can be divided into two classes: symbolic methods and non symbolic or iconic methods [1]. The first ones are based on segmented images and/or extracted features or salient points (following a SIFT or SURF algorithm for instance) [2,3,4,5,6]. The second ones are only based on pixel intensities and aim to establish a global relationship between the pixels of the two images using their gray levels only [7]. We proposed here a method of the second class that uses the Kullback-Leibler divergence to measure the similarity between the master and the slave sets of amplitude distributions of homogeneous areas.

2.2   Proposed method

Here the two images to be registered are geo-referenced and the basic linear transform to be estimated is a translation. Moreover the registration procedure aims to provide overlapped areas where changes in terms of contacts have to be found. In such a context, registration cannot be based on the contacts themselves but rather on pixel distributions of homogeneous areas. Hence we were interested in developing an iconic method for estimating the global translation that provides the best image matching in terms of homogeneous areas. For this the similarity between the master and the slave sets of amplitude distributions is computed using a global Kullback-Leibler divergence. These sets are carried out into two steps: two 3-staged image pyramids are first built. The first pyramid decomposition is needed to speed up the registration procedure and only consists in subsampling the image by a factor of 2 along each spatial dimension. Between stages of the second pyramid, besides subsampling, a median filtering is performed in order to denoise the

images. This allows performing a segmentation of the master image at the coarser stage into six homogeneous areas by applying the Fisher method which consists in minimizing the variance within classes [8]. The resulting segmented image is used in the remaining as a mask providing the six homogeneous areas. Note that even at the coarser stage the image size is sufficient for allowing a good estimate of the six distributions of pixel level.

At each stage of the first pyramid this mask is used to collect six pairs of pixel level distributions for a given translation of the slave image compared to the master image. Then a symmetric Kullback-Leibler divergence D_{KL} is computed for each pair of discrete distributions P and Q [9]:

$$D_{\mathrm{KL}}(\mathrm{P}||\mathrm{Q}) = \left[\sum_i \mathrm{P(i)}\log\left(\frac{\mathrm{P(i)}}{\mathrm{Q(i)}}\right) + \sum_i \mathrm{Q(i)}\log\left(\frac{\mathrm{Q(i)}}{\mathrm{P(i)}}\right)\right]/2 \text{ where } i \in [0,255]$$

The global Kullback-Leibler divergence for a given translation and for a given stage is the sum of the six symmetric Kullback-Leibler divergences. The estimated translation is the one that gives the lower global Kullback-Leibler divergence. At the coarser stage, the translation interval is bounded by the georeferencement accuracy. The estimated translation is used at the upper stage to initialize the new translation estimation bounded by only two pixels this time: this indeed corresponds to the subsampling factor between stages in rows and in columns. The global translation used for registering images is obtained by combining the translations estimated at every stage.

3   INCOHERENT CHANGE DETECTION

3.1   Log-ratio image

In the synthetic aperture radar (SAR) domain, image rationing pixel by pixel is performed for decades [10]. Ratio of images is preferred to difference because the ratio value only depends on relative change in amplitude between the two dates so that the detection of changes does not depend on the level of the pixels [11]. It is usually expressed in decibels (that is, by taking ten times the logarithm in base ten of the ratio of the intensities). This method aims to identify changes in the mean backscatter power of a scene. An estimate of the mean backscatter power is given by the pixel intensity. Moreover as the image is corrupted by speckle an averaging is required in order to ensure a good estimate [12]. Whereas the averaging is performed using N looks of the SAR data, we have to manage here with a single sonar look. Hence the two images are first processed by an average filtering using a sliding window. Moreover we deal with amplitude data, *i.e.* the square root of the intensity data: that induces a multiplication of the above ratio by two. Finally the log ratio of sonar images is given by:

$$Idiv = 20log_{10}\frac{<I_m>}{<I_s>}, \quad \text{where } <I_m> (resp. <I_s>) \text{ is the averaged master (}resp.\text{ slave) image.}$$

In order to detect any change whatever its origin we take the absolute value, *i.e.* $|Idiv|$. In this latter, pixel values over a given threshold are supposed to show a change in the backscattered energy. Here this threshold is fixed to the 99th percentile. In order to discard remaining false alarms in the thresholded image *Ib*, a binary morphological erosion is performed so that to keep objects as least as large than an object of size 30cm in azimuth and 50cm in range, this provides the image *Ibd*. Remaining detections are then processed individually: if the detected surface is not compact enough (proportion of the pixels in the convex hull that are also in the region must be over 0.7), it is rejected; otherwise we first perform a new but finer registration by cross-correlating the snippets corresponding to the area surrounding the detection in the master and the slave images, and then the new resulted log-ratio area is thresholded as above and the result compared to the previous one: no common pixel leads to a rejection.

3.2   Detection difference image

High-frequency sonar images suffer from a well-known multiplicative noise process that is commonly called *speckle* [13, 14]. When the number of scatterers in a resolution cell is sufficiently high, the pixel gray levels follow a Rayleigh law. Under this hypothesis, the ratio value between the standard deviation and the mean of pixels, called the coefficient of variation c_v, is constant and

equal to
$$c_v^{th} = \sqrt{\frac{4}{\pi} - 1} = 0.52$$

When this coefficient locally differs from the above theoretical value, it is probably due to an object that locally disturbs the distribution.

The idea is to locally estimate this coefficient in the master and slave images and to compare the two processed images. Practically, each sonar image is first divided into snippets that consist of rectangular patches corresponding to an area of 3m by 3m with an overlap of 75%. For each snippet, the coefficient of variation c_v is computed and all the pixel levels of the corresponding snippet are set to the coefficient value or, for overlapped snippets, the average coefficient of variation. Let us call Icv_m and Icv_s the two processed images.

Before differencing, we only keep pixels whose level is at least equal to $m_{Icvx}+2\sigma_{Icvx}$ (x=m or s) where m_{Icvx} (*resp.* σ_{Icvx}) is the average level (*resp.* the standard deviation) of the pixels of the entire processed image. Let us call It_m and It_s the two new images. The difference image $Itd = |It_m - It_s|$ is computed and normalised to one. In this image, we can see the main changes but some are false alarms. To discard them, a grey-level morphological opening with a structural element equivalent to an area of 1m in azimuth and 2m in range is performed: the resulting $Itdo$ image is normalised to one as well. A binary image $Itdob$ is then obtained by thresholding $Itdo$ to 0.7: remaining areas are detections. Each detection is processed individually: we first perform a new but finer registration by cross-correlating the snippets corresponding to the area surrounding the detection in the master and the slave images, and then the new difference area is thresholded as above and the result compared to the previous one: no common pixel leads to a rejection. A last test is performed in order to discard "ring-shaped" false alarms due to scale difference between detections: this test consists in verifying the central position of the hole in the ring.
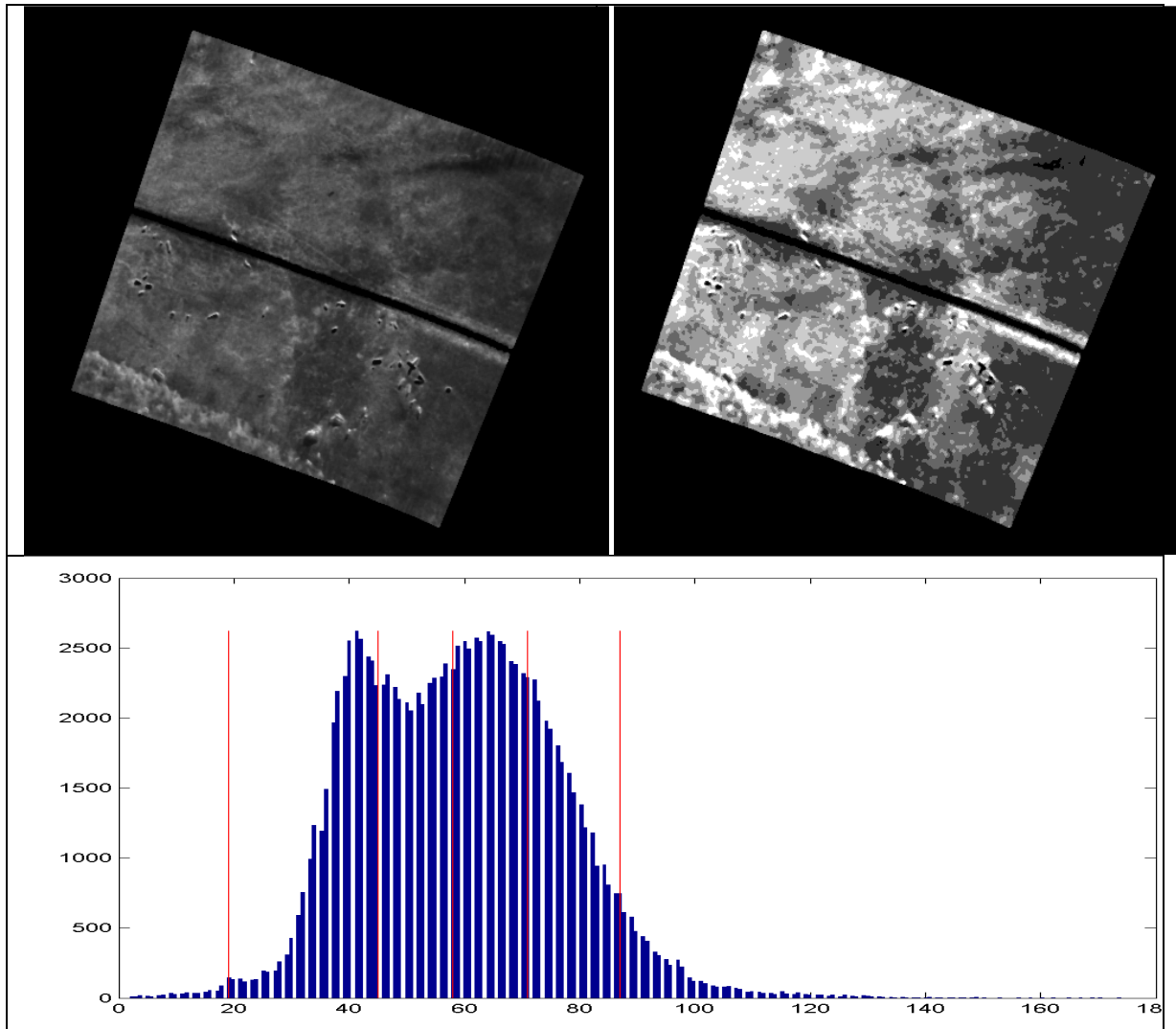

Figure 1 – First pair results. Left upper part: Filtered master image at the coarser resolution; Right upper part: segmented (6 classes) master image = mask; lower part: histogram of the filtered master image and the five thresholds (red lines) given by the Fisher method.

4   RESULTS

4.1   Data description

The data set was gathered with the Canadian Interim Remote Minehunting and Disposal System (IRMDS) which is a semi-submersible drone towing a Klein 5500 sidescan sonar operating at a centre frequency of 455 kHz and a bandwidth of 20 kHz. Two surveys were undertaken roughly one month apart during the winter of 2008 in a port area. Images were also normalised using a simple technique to remove effects of beam pattern, grazing angle and propagation loss and to create an image which is constant (in amplitude) with range. Finally, images were georeferenced on a grid with a resolution of 0.11m x 0.11m. Data samples falling into the same grid cell were averaged. See [15] for details. Here we will use only two image pairs among the five available ones:
- The first pair with many objects on the seafloor, some texture on the edges of the insonified area
- The second pair acquired during the vehicle turn (inducing distortion in the images), many objects and debris scattered on the seafloor with characteristic shapes.

4.2   Rigid-body registration

Intermediate results concerning the segmentation step are only given for the first pair in Figure 1. Figure 2 and Figure 3 give the registration results for the first and the second image pair.
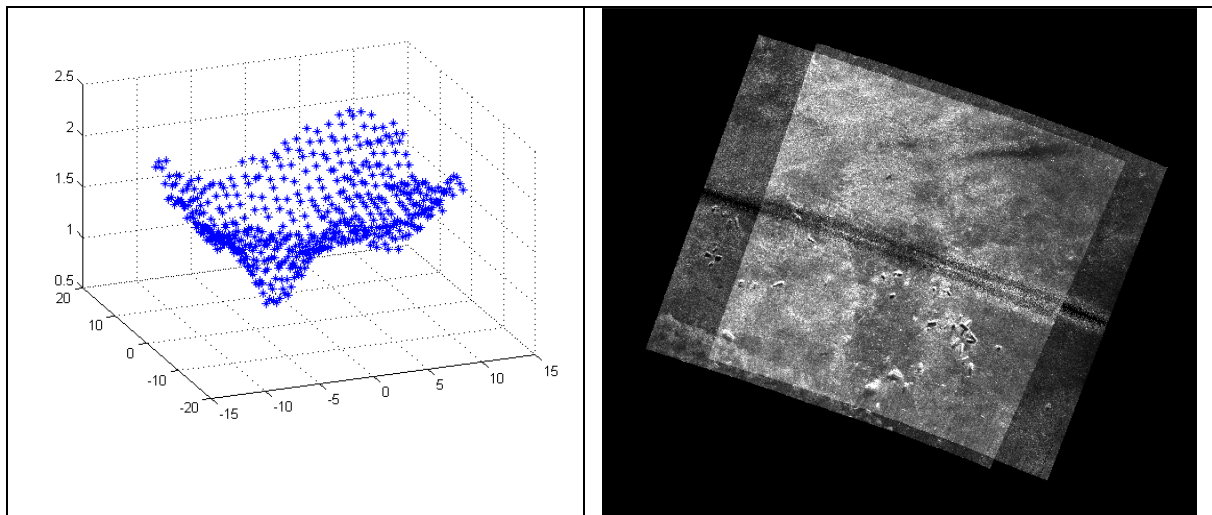

Figure 2 – Registration results for the first image pair: on the left, global Kullback-Leibler divergence *vs.* xy-translation at the coarser stage (the lower divergence indicates the good translation); on the right, superimposed registered images.
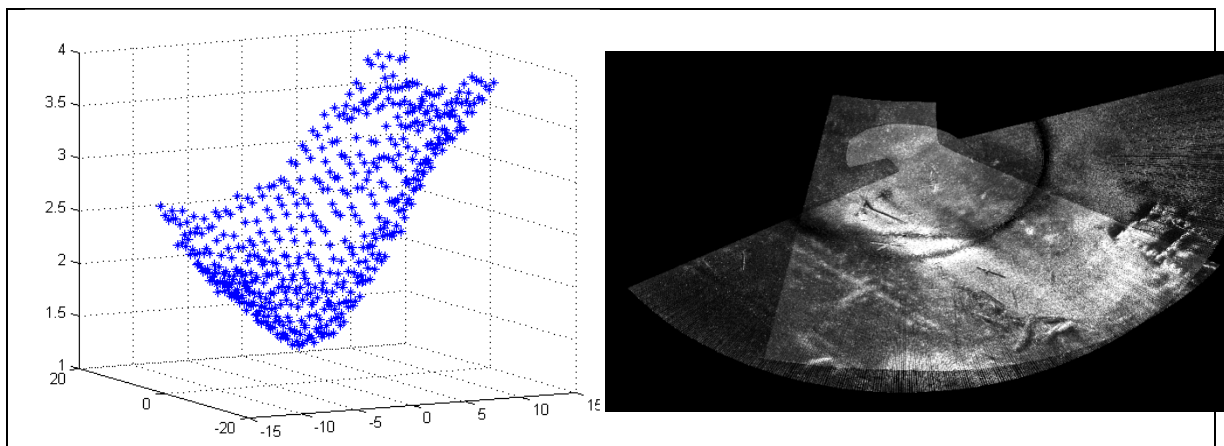

Figure 3 – Registration results for the second image pair: on the left, global Kullback-Leibler divergence *vs.* xy-translation at the coarser stage (the lower divergence indicates the good translation); on the right, superimposed registered images.
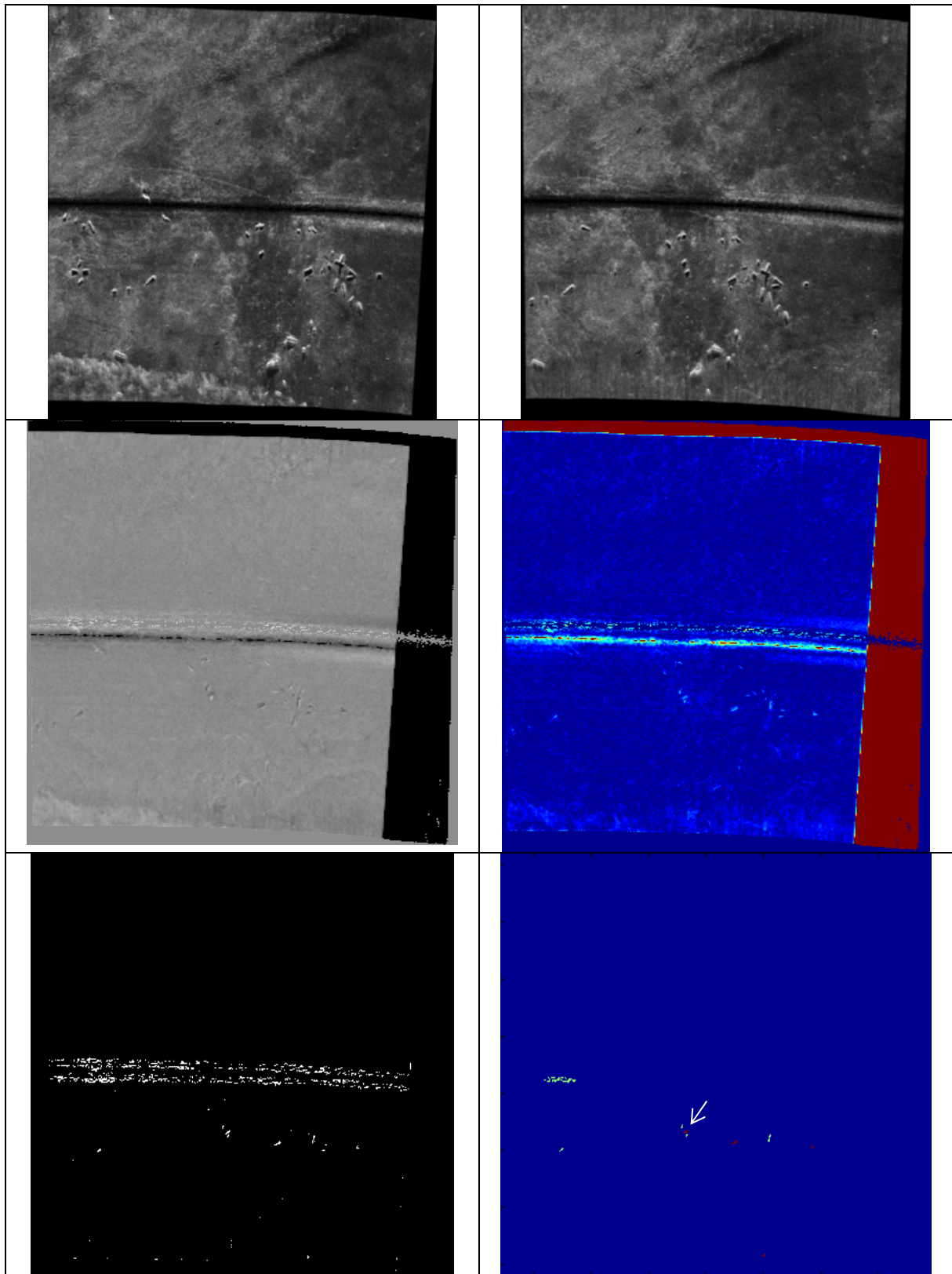
Figure 4 – First pair results for the log-ratio image method. Upper part: averaged images $<I_m>$ and $<I_s>$; Middle part : left figure $Idiv$, right figure $|Idiv|$; Lower part: left figure shows the thresholded image Ib and the right figure shows the four final detections in red (the added object is indicated by an white arrow) superimposed to the remaining detected objects in green after morphological operation Ibd.
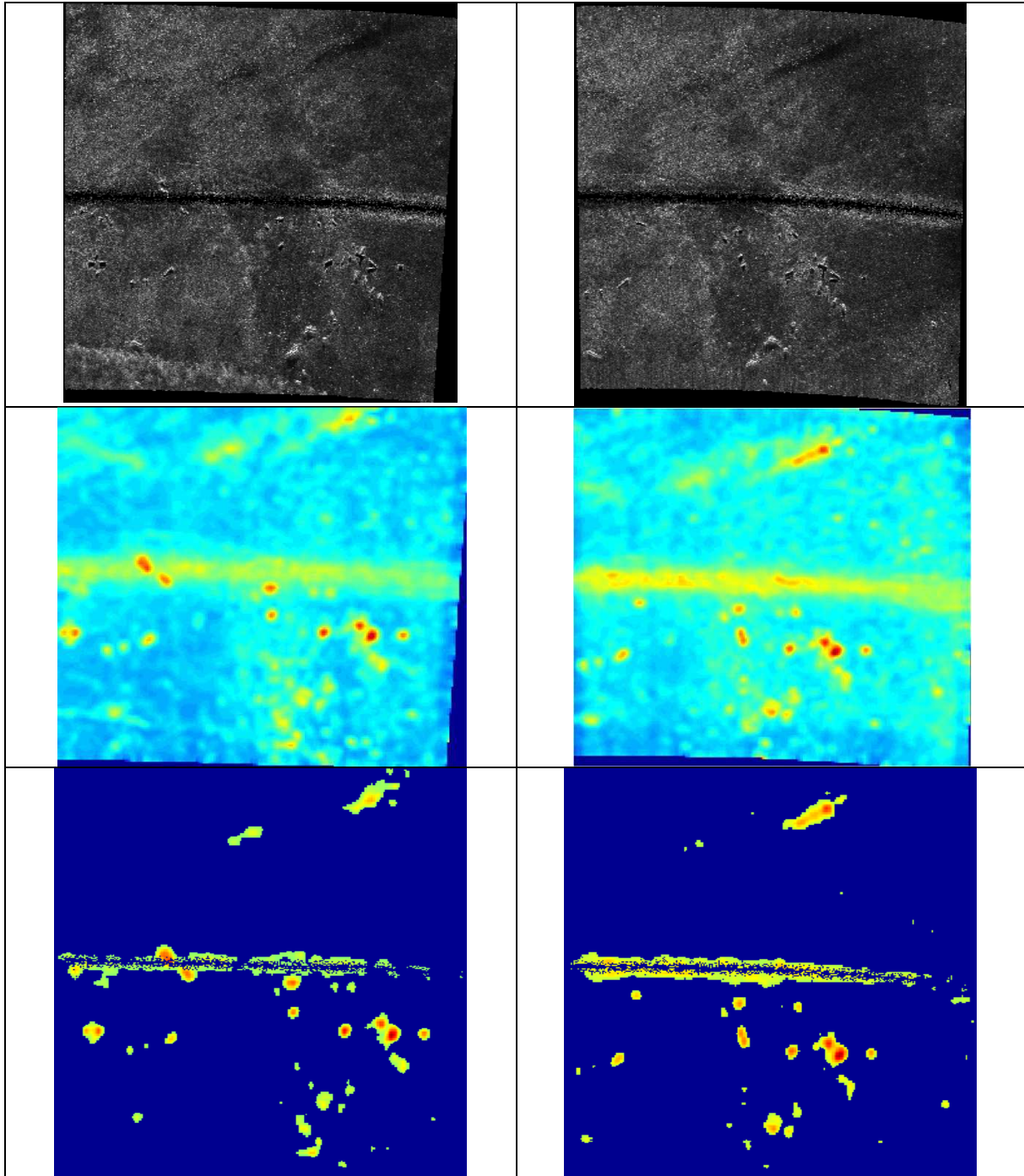
Figure 5 – First pair results. Upper part: sonar images (master one I_m on the left, slave one I_s on the right); Middle part: the processed image Icv_x (x=m or s) by computing the coefficient of variation; Lower part: It_x after having kept pixels whose level is at least equal to $m_{Icvx}+2\sigma_{Icvx}$.

4.3   Incoherent change detection

Both methods are assessed on the first image pair where several objects lay on the seafloor. An object has been added manually in the slave image in order to provide some ground truth. From now, the images are rotated so as to be able to adapt morphological structural elements in range and in azimuth.

4.3.1   Log-ratio image

Figure 4 shows successively the averaged images $<I_m>$ and $<I_s>$, the log-image ratio $Idiv$, its absolute $|Idiv|$, the thresholded image Ib and then, selected detections given the procedure detailed in section 3.1. The added object is well detected with 3 false alarms mainly due to broken objects.

4.3.2   Detection difference image

Figure 5 shows columnwise: the sonar image (master one I_m on the left, slave one I_s on the right), the resulted image after the computation of the coefficient of variation Icv_x (x=m or s), and then It_x after having kept pixels whose level is at least equal to $m_{Icvx}+2\sigma_{Icvx}$.

Figure 6 shows in the upper part the difference image before (Itd on the left) and after ($Itdo$ on the right) morphological opening. In order to compare these two images, they have been binarised by setting all non-zero pixels to one and then superimposed. The resulting image is showed in the left lower part of the figure whereas the right lower part shows the remaining detections following the procedure detailed in section 3.2. The added object is well detected with 3 false alarms due to image frontier or contrast change.
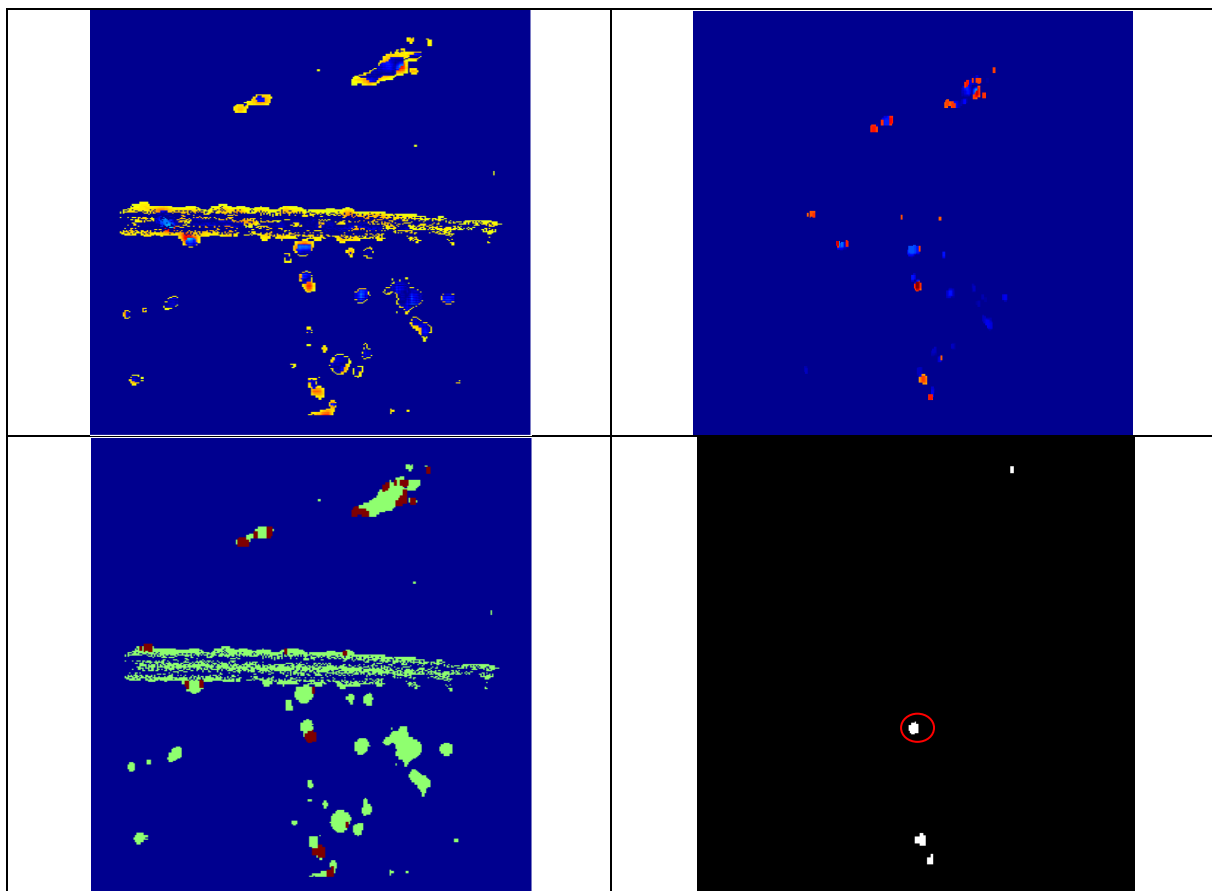

Figure 6 – First pair results for the detection difference image method. Upper part: difference image *Itd* on the left and after morphological grey-level opening *Itdo* on the right ; Lower part : on the left the superimposition of the images *Itd* (green) and *Itdo* (red) after a binarization and on the right the 4 remaining detected objects where the added object is encircled.

5   CONCLUSION

In this paper, the problem of incoherent change detection between two sonar passes has been addressed. Two methods have been proposed and applied to a set of amplitude sonar data gathered in a port area. Both proposed methods have similar performances in terms of change detection with a low false alarm rate. However, the log-image ratio is more sensitive to small changes as shape distortion than the second method based on the difference of values corresponding to the coefficient of variation C_v. Indeed whereas the first is a low level processing that compares (averaged) images pixel by pixel, the second compares the high level information returned by a C_v computer.

ACKNOWLEDGEMENTS

REFERENCES

1. C. Chailloux, *Recalage d'images sonar par appariement de régions. Application à la génération d'une mosaïque*, PHD thesis, ENST Bretagne, Brest, June 2007.
2. D. Gueriot, E. Maillard, and J.-P. Kernin, "Sonar image registration through symbolic matching: A fuzzy local transform approach using genetic algorithms," in Proc*. MTS/IEEE OCEANS Conf.*, Sep. 1996, vol. 3, pp. 1324–1329.
3. S. Daniel, F. Le Leannec, C. Roux, B. Solaiman, and E. Maillard, "Side-scan sonar image matching," *IEEE J. Ocean. Eng.*, vol. 23, no. 3, pp. 245–259, Jul. 1998.
4. P.Y. Mignotte, M. Lianantonakis, and Y. Petillot, **"**Unsupervised registration of textured images: applications to sidescan sonar**"**, *Oceans 2005 – Europe,* 2005.
5. I. Leblond, *Recalage à long terme d'images sonar par mise en correspondance de cartes de classification automatique des fonds*, PHD thesis*,* Université de Bretagne Occidentale, ENSIETA, Brest, February 2006.
6. S. Daniel and M. Bach, *Automatic Image Co-registration Study for Sidescan Sonar*, Contract Report, DRDC Atlantic CR 2010-022, January 2010.
7. C. Chailloux and B. Zerr, « Non Symbolic Methods to register SONAR images », *Oceans 2005 – Europe,* 2005.
8. W.D. Fisher, "On grouping for maximum homogeneity", *American Statistical Association Journal*, vol. 53, pp789-798, 1958.
9. S. Kullback, *Information theory and statistics*, John Wiley and Sons, NY, 1959.
10. A. Singh, "Digital change detection techniques using remotely sensed data," *Int. J. Remote Sensing***,** vol. 10, pp. 989-1003, 1989.
11. E. Rignot and J. Van Zyl, "Change Detection Techniques for ERS-1 SAR Data", *IEEE Transactions on Geoscience and Remote Sensing*, Vol. 31, No. 4**,** July 1993.
12. M. Preiss and N. Stacy, *Coherent Change Detection: Theoretical Description and Experimental Results*, technical report DSTO–TR–1851, August, 2006.
13. J. S. Lee, "Statistical modeling and suppression of speckle in synthetic aperture radar images", in *Proc. of IGARSS'87*, pages 1331-1339, Ann Arbor, 18-21 May 1987.
14. F. Schmitt, L. Bonnaud and C. Collet, "Contrast control for sonar pictures", Signal and Image *Processing, SPIE'96 – Technical Conference on Application of Digital Image Processing XIX*, vol. 2847, pp. 70-82, Aug. 1996.
15. V. Myers, *A data set for change detection in port environments using sidescan sonar*, Technical memorandum, DRDC Atlantic TM 2008-247, 2009.